CRYSTAL GROWTH & DESIGN

pubs.acs.org/crystal

Article

Influence of Monounsaturated Triglycerides on the Crystallization Pathway of Fully Saturated Triglycerides

Julia Seilert,* Michael Rappolt, Georg Dol, and Eckhard Flöter

Cite This: *Cryst. Growth Des.* 2024, 24, 9951−9964

Read Online

ACCESS | Metrics & More | Article Recommendations | Supporting Information

ABSTRACT: The effect of composition on the polymorphic crystallization in blends of fully saturated and monounsaturated triglycerides was investigated (H3 denotes fully saturated, and H2U denotes monounsaturated triglycerides). Fully hydrogenated rapeseed oil (FHRO) and palm oil stearin (POSt) were used as H3 sources. Palm oil (PO) served as an H2U source. Different H3/H2U ratios and cooling rates (1, 5, and 10 °C min^{-1}) were investigated. Differential scanning calorimetry, time-resolved small- and wide-angle X-ray scattering, and oscillatory shear experiments were employed to investigate the melting behavior as well as the nano- and microstructural development. The data reveal different kinetic pathways, even selective cocrystallization, depending on the molecular makeup of the H3 fraction. The POSt-PO blends first crystallize in an α phase that transitions into coexisting β' and β phases. The FHRO-PO blends showed a longer persisting α phase that transitions into β even before a β' phase could be identified. This indicated separate crystallization of H3 triglycerides. The polymorphic pathways are compared to the melting behavior and microstructural development during crystallization. Further, the question of mixed crystal formation in the H3 fraction of the FHRO-PO blends was addressed by studying H3 blend replicates in the absence of H2U triglycerides. This paper is the second part of a series investigating the interplay of polymorphic transition and mixed crystal formation.

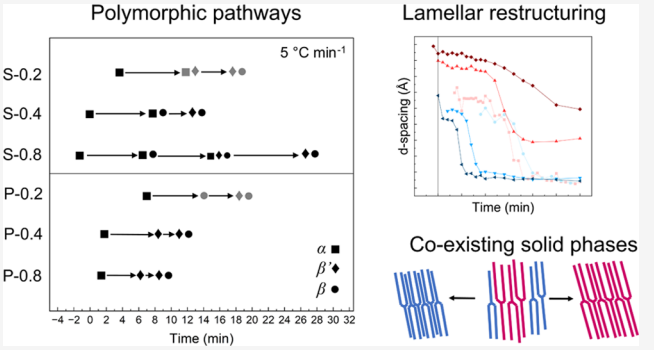

1. INTRODUCTION

The polymorphic crystallization of structuring fats plays an important role in product development and can be utilized to alter melting properties, plasticity, and stability, i.e., phase separation and phase interface stabilization. The crystallization behavior of such structuring fats can be directed by internal factors such as triglyceride (TAG) composition and process parameters such as cooling rate, temperature, and shear.[1] In the crystallization process, multiple phases may be formed varying in the stability of the polymorphic form and composition. While the first is essentially a function of the applied driving force, i.e., supersaturation, the latter is dictated by the mixture's phase behavior, i.e., the likelihood of co- or separate crystallization.[2] In other words, during this process, the interplay of changing driving forces and crystallization kinetics may cause situations of segregation of actually miscible components.

A natural fat, rich in structuring triglycerides, is palm oil (PO). PO has a characteristic content of 5−7% monoacid saturated TAGs, namely tripalmitin (decoded using a three-letter code as PPP). In addition 35−40% monounsaturated TAGs, mainly 1,3-dipalmitoyl-2-oleoyl-*sn*-glycerol, 1,2-dipalmitoyl-3-oleoyl-*sn*-glycerol, and POP and PPO render PO an exceptional oil.[3] It is known to exhibit a complex crystallization behavior, including multiple mixed solid phases and the formation of molecular compounds (MC).[4] This complicates not only the separation processes to reach high-purity fractions during fractionation but also its replacement in fat-continuous products. PO's replacement is an ongoing effort driven by consumer concerns about the sustainability of PO. In general, this necessitates the understanding of the kinetic pathways. It is noteworthy that the resulting crystallization behavior oftentimes deviates significantly from what equilibrium phase behavior suggests.[2]

Using PO as a model fat, its multistep crystallization was a subject of numerous studies that reported either a two-step process (at low temperatures) or a one-step process (at high temperatures).[5−9] In both, calorimetric and rheological studies it was postulated that the two-step process is caused by the formation of an α polymorph that undergoes a transition into a β' polymorph.[5] In various shear-dependent studies, the transition of an α-phase into a β'-phase seemed to be

Received: August 14, 2024
Revised: November 13, 2024
Accepted: November 13, 2024
Published: November 21, 2024

enhanced by applying shear[9−11] and modifiable via the applied cooling rate.[12] The crystallization of PO's higher-melting fraction is largely driven by PPP, however, the formation of β'-2L PPP crystals is limited, since it is significantly affected by shear. In contrast, the formation of the lower-melting α-2L POP and of the molecular compounds of high-melting TAGs POP, PPO, and PPP in the β'-2L phase are easily promoted.[13] A recent study on the mixing behavior of PPP and the prominent molecular compound $MC_{POP/PPO}$ shows that the molecular compound itself acts as a pseudopure component forming an "eutectic" mixture with PPP.[14]

PO is no exception displaying cocrystallization (or mixed crystal formation) and separate crystallization. Also anhydrous milk fat, an even more complex TAG mixture, exhibits multiple-step crystallization facilitated by shear.[15−18] Other authors[18] highlighted the effect of different TAG melting points on the kinetic pathways. Despite crystallizing as well, the low-melting fraction of TAGs was assumed to act as a solvent for high-melting TAGs. Observations again depend on supersaturation and kinetics, resulting in different crystallization rates of the fractions as described earlier.[19]

Generally, the findings summarized above highlight the complexity in (kinetic) phase behavior, i.e., cocrystallization and segregation, accompanied by polymorphic transitions. It is necessary to consider systems that either show solid miscibility/cocrystallization over the complete concentration and temperature range considered with recrystallization exclusively due to polymorphic transitions or systems that segregate during crystallization (limited miscibility) such that the occurrence of multiple solid phases and polymorphic transitions are superimposed.

This contribution is the second part of a series describing our systematic studies on crystallization pathways, particularly polymorphic transitions as a function of the TAG composition in complex fat blends.[20] In brief, TAGs are classified into four main melting groups: H3, H2M, H2U, and HM2. H denotes a long-chain saturated fatty acid exceeding 16 carbon atoms, M denotes a medium-chain saturated fatty acid of either 12 or 14 C atoms, and U denotes any unsaturated fatty acid. The asymmetry of TAGs is not accounted for; i.e., HUH and HHU are summed up as H2U. In this contribution, the effect of composition was studied by the variation of both the ratio of H3 to H2U TAGs and the source of H3 TAGs—being fully hydrogenated rapeseed oil (FHRO) or palm stearin (POSt). PO was the H2U source. It must be noted that since PO itself contains about 7% H3 TAGs, the H3 fraction in the system FHRO-PO is in fact a mixture of mostly tristearin (SSS) and tripalmitin (PPP).

The crystallization route under quiescent conditions was investigated by DSC, time-resolved small- and wide-angle X-ray scattering (SAXS/WAXS) experiments. Oscillatory shear experiments were performed to observe the melting behavior and nano- and microstructural development. This study aims to correlate polymorphic pathways to the blends' composition and the effect of H2U on the polymorphic crystallization of H3 triglycerides. Possible mixed crystal formation in early-stage crystallization is discussed. In contrast to comparable studies, a relatively high temperature was chosen. This way, the crystallization of lower-melting TAG groups (HU2 originating from the PO) is avoided. Additionally, the relatively low supersaturation of the high-melting TAG group (H3) slowed the nucleation processes to be captured during the experiments.

2. MATERIAL AND METHODS

2.1. Material. FHRO was kindly provided by ADM (Hamburg, Germany). Refined, bleached, and deodorized PO was contributed by Flora Food R&D B.V. (Wageningen, The Netherlands). The PO has a comparable DAG content as found in other industrial PO, approximately 6−8%.[21] Multiple fractionated palm stearin (POSt) with an iodine value of 12 was kindly provided by AAK (Aarhus, Denmark). Refined rapeseed oil (RP) was contributed by Gustav Heess GmbH (Leonberg, Germany). Tripalmitin (PPP) with a purity of >98% was purchased from ThermoScientific (Dreieich, Germany). All materials were used without further modification.

2.2. Fat Blend Formulation. The interplay of H3 and H2U triglycerides was studied by varying the ratios of these triglycerides. Furthermore, two H3 sources, POSt, and FHRO, were studied. The samples are denoted as S-0.2 (P-0.2), S-0.4 (P-0.4), and S-0.8 (P-0.8), where S (FHRO) and P (POSt) denote H as primarily either stearic or palmitic acid in the H3 TAGs. The H3 to H2U ratio in the samples is set to 0.2, 0.4, and 0.8, respectively. PO was the main H2U source. The H3 originating from POSt is dominated by tripalmitin PPP. FHRO consists mostly of SSS, SSP and PSP, deduced from the fatty acid profile (see ref 20). The H3 sources were mixed with PO, which is generally known to consist of: 5.1% PPP, 1.2% PPS, 0.3% PSP (total H3 = 7.4%),[4] and 35−40% POP/PPO (H2U group).[3,4] This renders the POSt-PO mixtures to consist of mostly palmitic-based triglycerides. Table 1 gives the fatty acid profiles of the blends determined from the information provided by the supplier of the raw materials. Table 2 summarizes the TAG groups of each blend.

Table 1. Fatty Acid Composition

fatty acid	S-0.2	S-0.4	S-0.8	P-0.2	P-0.4	P-0.8
C14:0	1.1	1.0	0.9	1.1	1.0	0.9
C16:0	44.2	41.1	37.2	45.7	48.6	52.2
C16:1	0.2	0.2	0.2	0.2	0.2	0.2
C18:0	6.0	12.9	21.4	4.3	4.5	4.6
C18:1	37.2	34.2	30.5	37.4	35.2	32.5
C18:2	10.0	9.3	8.3	10.0	9.3	8.5
C18:3	0.2	0.2	0.2	0.2	0.2	0.2
C20:0	0.4	0.6	0.7	0.4	0.4	0.3
rest	0.7	0.6	0.6	0.7	0.7	0.7

In the FHRO-PO mixtures, the H3 fraction is primarily a mixture of SSS (from FHRO) and PPP (from PO). Note, the composition of blend S-0.2 is close to that of straight PO. The interaction of PPP with the H3 TAGs originating from FHRO in the blends S-0.2, S-0.4, and S-0.8 was studied explicitly in absence of H2U TAGs. Therefore, the respective H3 fractions were replicated with pure PPP (>98% purity) and FHRO (>97.8% stearic-dominated saturated triglycerides) and diluted with rapeseed oil to match the H3 level (9.6, 17.0, 26.2%, see Table 2) and the ratio of SSS:PPP. The ratios of SSS and PPP are summarized in Table 3. In the S-0.2 and H3(S-0.2) blends, the PPP outweighs SSS due to PO's high content of PPP.

All blends were prepared by melting the materials and keeping them at 80 °C for at least 15 min. Prior to blending, samples were stirred to ensure homogeneity. Since all experimental procedures started from liquid samples, any crystallization because refrigerated storage was considered uncritical.

2.3. Methods. *2.3.1. Calorimetry.* A 214 Polyma calorimeter (Netzsch, Selb, Germany) was used to perform differential scanning calorimetry (DSC) experiments. The sample size was 10−15 mg, weighed in aluminum crucibles, and sealed hermetically. An empty crucible was used as a reference. Initially, samples were kept for 10 min at 80 °C to remove any crystal memory. Subsequently, cooling to 25 °C was performed at 10 °C min^{-1}. Stabilization at 25 °C was allowed to proceed for 30 min. Samples were heated to 80 °C at a rate of 2 °C min^{-1}. The H3(SSS:PPP) subsystems were crystallized similarly. Peak temperatures were analyzed using the manufacturer's software. All measurements were performed in duplicate.

https://doi.org/10.1021/acs.cgd.4c01138
Cryst. Growth Des. 2024, 24, 9951−9964

Table 2. Triglyceride (TAG) Melting Group Contents in Blend in Percentages[a]

TAG melting group	S-0.2	P-0.2	S-0.4	P-0.4	S-0.8	P-0.8
H3	9.6	9.7	17.0	17.0	26.2	26.0
H2M	1.3	1.3	1.2	1.1	1.0	0.9
H2U	42.2	42.2	38.7	39.3	34.4	35.8
H3/H2U	0.2	0.2	0.4	0.4	0.8	0.7
sum H3 + H2M + H2U	53.0	53.2	56.8	57.5	61.6	62.8
H2Sh	0.0	0.0	0.0	0.0	0.0	0.0
HM2	0.0	0.0	0.0	0.0	0.0	0.0
M3	0.0	0.0	0.0	0.0	0.0	0.0
M2U	0.0	0.0	0.0	0.0	0.0	0.0
HMU	3.7	3.7	3.4	3.3	3.0	2.8
HU2	34.2	34.0	31.4	30.6	27.9	26.5
MU2	1.5	1.4	1.3	1.3	1.2	1.1
U3	7.5	7.6	6.9	7.2	6.2	6.7
rest	0.00	0.00	0.00	0.01	0.04	0.08

[a]H—long-chain saturated fatty acid > C14:0, M—medium-chain saturated fatty acid C12:0 and C14:0, Sh—short chain saturated fatty acid < C12:0, U—unsaturated fatty acid. S or P denotes the H3 source and 0.2, 0.4, and 0.8 give the H3/H2U ratio of the samples.

Table 3. Ratio of Tristearin and Tripalmitin (SSS:PPP) in the H3 Blends Imitating the H3 Fraction in the S-0.2, S-0.4, and S-0.8 Blends

	H3(S-0.2)	H3(S-0.4)	H3(S-0.8)
SSS:PPP ratio	21:79	59:41	76:24

2.3.2. Rheology. An MCR 302 rheometer (Anton Paar GmbH, Graz, Austria) was used to perform small deformation oscillatory experiments. The instrument was equipped with a sandblasted parallel plate geometry (PP50, d = 50 mm, initial gap height = 0.4 mm). The normal force was set to zero to allow the instrument to compensate for sample contraction by adjusting the gap distance. For all samples, the complex modulus $|G^*|$ was monitored during cooling from 70 to 25 °C at 10 °C min^{-1} and the isothermal stabilization phase. All tests started with a molten sample, that was loaded onto the preheated Peltier plate (T = 70 °C) and allowed to stabilize for 5 min applying mild shear ($\dot{\gamma}$ = 1 s^{-1}). During the cooling and isothermal step a constant strain of γ = 0.01% and an angular frequency 10 rad/s were applied. The strain was sufficiently low, ensuring that the experiments were performed in the linear viscoelastic region, which was confirmed by a previously performed amplitude sweep on a highly crystalline sample (S-0.8). The isothermal temperature of 25 °C was chosen to capture the crystallization kinetics of high-melting TAGs, i.e., H3, in the presence of H2U triglycerides. Each experiment was performed in duplicate.

2.3.3. X-ray Scattering Measurements and Analysis. A SAXSpace instrument (Anton Paar GmbH, Graz, Austria) was used to perform simultaneous SAXS and WAXS measurements. The instrument operates at 40 kV and 50 mA and uses a Cu anode (λ = 0.154 nm). The sample−detector distance was set to 130 mm which covers a q range from 0.1 to 17.6 nm^{-1} ($q = 4\pi(\sin\theta)/\lambda$, with 2θ being the scattering angle). The 1D scattering patterns were recorded with a Mythen microstrip X-ray detector (Dectris Ltd., Baden, Switzerland). Temperature control was achieved with a Peltier element of TCstage 150 (Anton Paar GmbH, Graz, Austria). Each sample was prepared in a quartz disposable capillary with an outside diameter of 1.5 mm (Capillary Tube Supplies Ltd., Cornwall, U.K.). In each experiment, the samples were subject to temperature protocols similar to those for DSC and rheology measurements. The molten sample (at 70 °C stabilized for 10 min to erase any crystal memory) was cooled to 25 °C at 1, 5, or 10 °C min^{-1} and subsequently held for 30 min isothermally. During the isothermal phase, exposure times of 30 s were applied every minute, guaranteeing an optimum counting rate. Continuous data collection during the cooling period was not possible. X-ray patterns were recorded, applying a step-function temperature profile resulting in a cooling rate of 5 °C min^{-1}. The sample was first cooled to a temperature of 35 °C and data were collected for 30 s. Subsequently, the sample was cooled down by 5 °C at a cooling rate of 15 °C min^{-1}, and held for 10 s, after which a frame was acquired again for 30 s exposure time. The procedure was repeated until the temperature of 25 °C was reached. When a cooling rate of 10 °C min^{-1} was used, the X-ray patterns were acquired basically in the same manner, except for using a shorter exposure time of 10 s. That is to achieve the desired effective cooling rate, the counting rate is nearly 2-fold lower, but still sufficient for identifying polymorphs unambiguously.

The primary beam position was set to zero, and the patterns were normalized for X-ray flux fluctuation and sample transmission using the SAXSTreat (Anton Paar GmbH, Graz, Austria) and SAXSQuant software (Anton Paar GmbH, Graz, Austria), respectively. The normalized pattern of an empty capillary was subtracted from that of each normalized sample pattern. Subsequently, the liquid contribution was subtracted. The resulting patterns were smearing mostly affecting the small-angle region, approximately from q = 0 to 2.5 nm^{-1} due to the line collimation focus of the instrument. OriginPro 2022b was used to perform peak analysis in the WAXS region. MATLAB 2020b was used to determine the d-spacing from the first-order reflection in the SAXS region as well as the area under the first reflection (integrated intensity). For determining the crystalline fraction as a function of time, first the diffuse scattering distribution was subtracted from each X-ray pattern, giving the pure diffraction contribution, i.e., resulting in SAXD/WAXD. Second, the diffracted intensity over the first-order region from 0.6 to 1.8 nm^{-1} was determined to display the trend of the crystalline fraction in each blend. For better comparison, all turnover curves were normalized to 1 at the end of the isothermal period (t = 30 min). Details on the subtraction of the liquid contribution and peak analysis can be found in the Supporting information in Figures S1−S3.

3. RESULTS AND DISCUSSION

In this study, the crystallization kinetics of H3 and H2U-containing blends were investigated. The effect of composition was studied by modifying the ratio of H3 to H2U TAGs (0.2, 0.4, and 0.8) and the H3 source (FHRO or POSt).

3.1. Calorimetric Study of the Mixing Behavior of SSS and PPP in the H3 Group. To elucidate the interaction of SSS (in FHRO) and pure PPP in the FHRO-PO system, the H3 fraction was recreated using pure PPP (>98% purity) and FHRO to match the amount in the blend (9.6, 17.0, and 26.2%, Table 2). Figure 1 shows the melting profiles of the H3 system.

https://doi.org/10.1021/acs.cgd.4c01138
Cryst. Growth Des. 2024, 24, 9951−9964

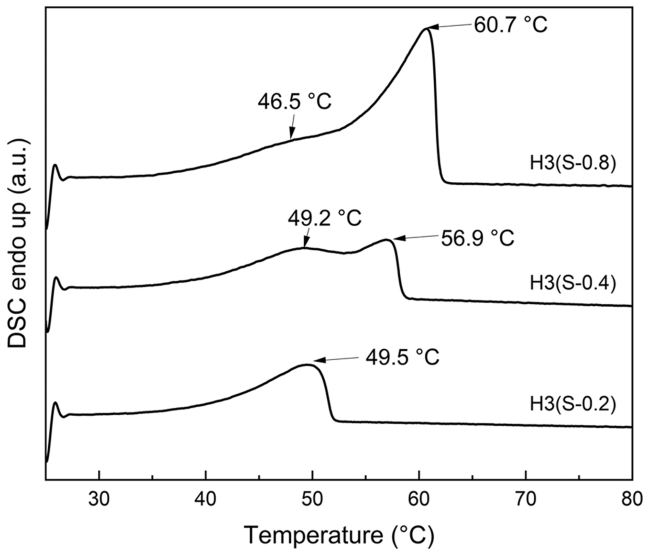

Figure 1. DSC melting curves of the H3(S-0.2), H3(S-0.4), and H3(S-0.8) blends with increasing SSS:PPP ratios of 21:79, 59:41, and 76:24, respectively. The scan rate was 2 °C min^{-1}. Cooling rate 10 °C min^{-1}. Melting peaks are indicated with arrows.

The blend with the lowest concentration, H3(S-0.2) (ratio of 21:79, ∼2% SSS) shows a single melting peak at 49.5 °C, whereas the higher concentrated blends show two melting peaks indicating demixing. The higher melting peak can be assigned to the SSS fraction increasing with the FHRO dosage. With increasing amounts of SSS, the amount of PPP decreases in the series from 7.6 to 7 and 6.2% in H(S-0.4) and H3(S-0.8), respectively, which explains the decrease in lower-melting peak temperature to 49.2 and 46.5 °C, respectively. The single melting peak observed for H3(S-0.2) might indicate a mixed H3 crystal. Likewise, the thermogram could be due to two overlapping peaks. Calculating the ideal pure component solubilities (Hildebrandt equation) reveals very similar dissolution temperatures for the given concentrations, 53.6 °C for SSS and 52.1 °C for PPP, in the respective β-polymorph.

Figure 2 gives the time-resolved DSC signal during the cooling and isothermal phase. Two crystallization steps for each sample can be observed, with the first event being more pronounced with increasing SSS concentration. The second crystallization peak observed does not change drastically when comparing blend H3(S-0.4) to H3(S-0.8).

The cooling curves confirm in the first place that irrespective of the composition of the H3 fraction, more H3 results in higher crystallization temperatures. The two-step crystallization is in line with a previous study of this lab investigating the crystallization of a stearic-based H3 system.[20] Specifically, a blend of comparable amounts of H3 (10 vs 9.6% in H3(S-0.2)) also showed two crystallization peaks, the first recorded at 0.08 min and the second recorded 1.12 min after the start of the isothermal hold. The timing of the events is comparable to that of the H3(S-0.2) blend of this study. For the two other blends, H3(S-0.4) and H3(S-0.8), SSS is the dominant TAG within H3 and hence crystallizes first (higher melting point and higher concentration). The second crystallization peak seems less affected by the change in SSS concentration and is hence assigned to PPP, whose concentration practically does change only between the three samples.

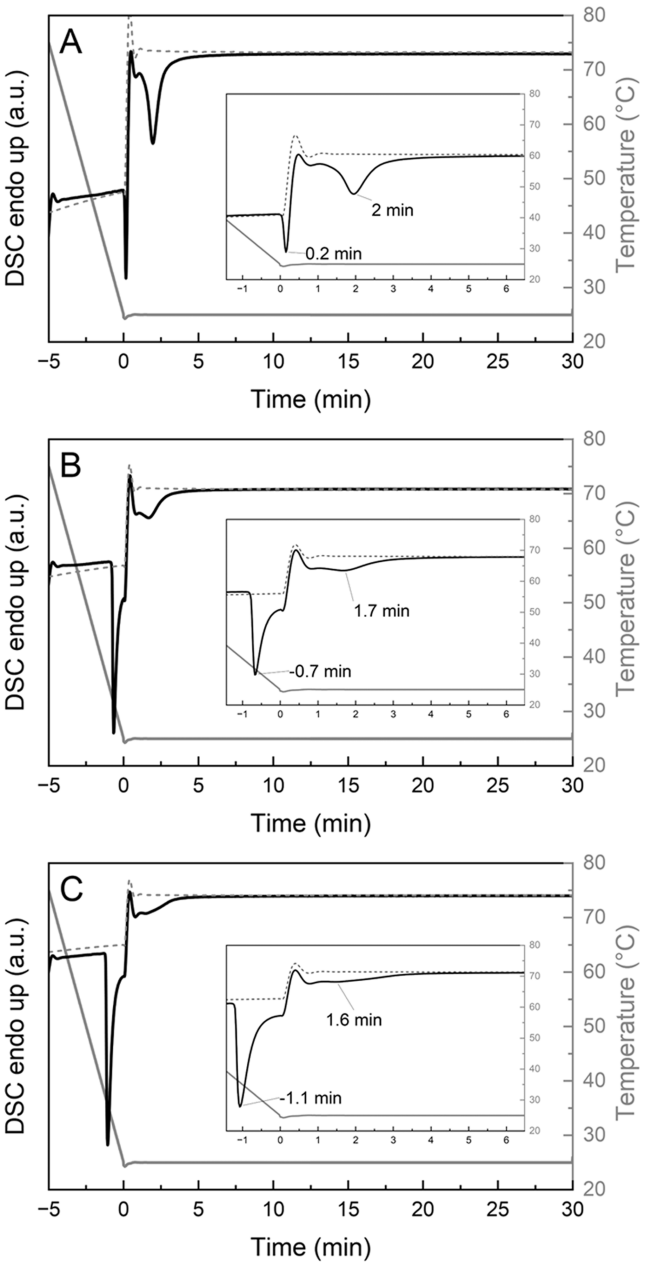

Figure 2. Isothermal DSC signal during crystallization and isothermal holding time of H3(S-0.2) (A), H3(S-0.4) (B), and H3(S-0.8) (C) all as solid lines. Inlay graphs show zooms, and additionally, the DSC signal obtained for rapeseed oil without any hardstock added (gray-dashed line) for reference. Cooling rate: 10 °C min^{-1}.

The observed melting and crystallization behavior of the H3 blends can be compared with the reported phase behavior of the binary SSS/PPP mixture. As pure components, SSS and PPP (both monoacid TAGs) undergo a direct polymorphic transition from the α into the most stable form β,[22,23] also observed for pseudopure FHRO. PPP also transforms into the β' phase, which is rather short-lived and oftentimes not observed.[24] The phase behavior of the binary system SSS/PPP is eutectic in the most stable polymorphic form β with a eutectic point around 20% of SSS.[25] The mixture is considered to be miscible in less stable polymorphic forms, α and β', given fast cooling rates are applied.[26] At lower cooling rates, however, mixtures with SSS concentrations in excess of 30% SSS show two separate α-phases, PPP- and SSS-rich,

https://doi.org/10.1021/acs.cgd.4c01138
Cryst. Growth Des. 2024, 24, 9951−9964

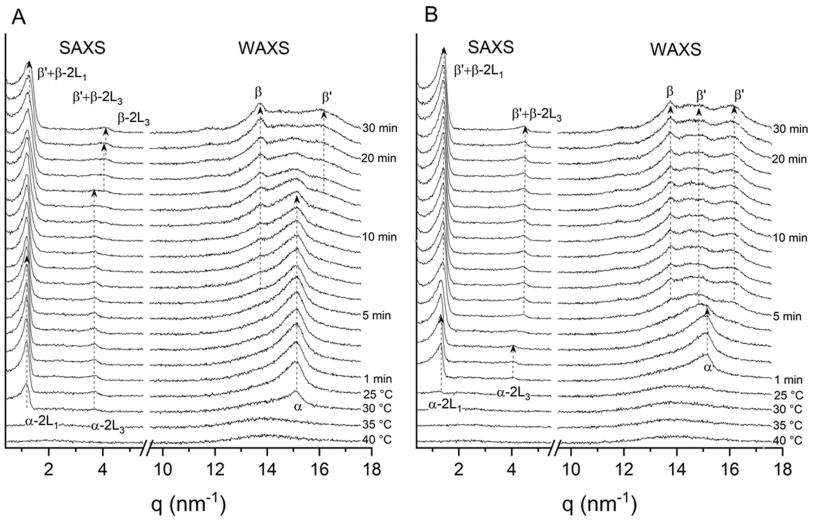

Figure 3. SAXS and WAXS patterns after subtraction of the liquid contribution (obtained at 70 °C) of S-0.8 (A) and P-0.8 (B) during cooling at 5 °C min^{-1} to 25 °C and subsequent isothermal holding time of 30 min. 1st and 3rd order reflections in the SAXS region and reflections in the WAXS region are indicated as identified.

Table 4. Summary of Long (SAXS Region) and Short Spacings (WAXS Region) of S-0.8 and P-0.8 Crystallized at 5 °C min^{-1}[a]

	temperature (°C)	time (min)	long spacing (Å)	short spacings (Å)		
			S-0.8			
α	30	−1	50.90	4.15 (vs)		
$\alpha + \beta$	25	6	50.25	4.61 (vw)	4.14 (vs)	
$\alpha + \beta$	25	10	49.99	4.61 (s)	4.13 (vs)	
$\alpha + \beta' + \beta$	25	12	49.79	4.58 (s)	4.13 (vs)	3.87 (vw)
$\beta' + \beta$	25	20	48.42	4.57 (s)	4.18 (w)	
$\beta' + \beta$	25	30	46.95	4.60 (s)	3.9 (w)	
			P-0.8			
α	25	1	46.45	4.15 (s)		
β'	25	4	46.00	4.22 (s)		
β'	25	5	45.37	4.55 (w)	4.25 (vw)	3.89 (m)
$\beta' + \beta$	25	20	42.43	4.58 (s)	4.20 (w)	3.89 (m)
$\beta' + \beta$	25	30	42.48	4.58 (s)	4.22 (m)	3.89 (m)

[a]vs, very strong; s, strong; m, medium; w, weak; vw, very weak.

respectively.[27,28] This renders the kinetic pathway of the binary mixture dependent on the cooling rate and the concentration. The blends of FHRO and PPP considered in this work were diluted with rapeseed oil to match the SSS:PPP ratio of blends H3(S-0.4) and H3(S-0.8). Given the elevated temperature, rapeseed oil acts as the solvent and does not contribute as the cocrystallizer to the solid phase forming. Hence, the mixing behavior in the solid phase is not affected by the rapeseed oil. However, minor components present in the oil can delay any crystallization and polymorphic transition. The experimental conditions of this study consequently suggest the formation of two α-phases transitioning separately into two β-phases for blends H3(S-0.4) and H3(S-0.8).

Regarding H3(S-0.2), it has to be noted that its SSS/PPP ratio of 21:79 hints toward crystallization that is dominated by PPP. Considering the binary PPP−SSS system with the eutectic concentration close to 20% SSS in the β polymorph, the first crystallization event is assigned to a mixed α-phase. Interestingly, the second crystallization event (at 2 min) is assumed to be the crystallization of PPP in the β polymorph, similar to the behavior of the two other samples. This means a segregation of PPP and SSS on polymorphic transition takes place. Concerning the fate of the 2% SSS in sample H3(S-0.2), two possible interpretations can currently not be distinguished. Either the small amount of SSS crystallizing was not observed during isothermal holding (Figure 2) this was observed in the earlier study—or the SSS is not crystallizing under the given circumstances. Consequently, the melting peak observed in Figure 1 is either due to two separate but overlapping β-phases (PPP and SSS, respectively) or exclusively due to PPP melting.

In summary, already the subsystems, H3 TAGs in the FHRO-PO blends, show a complicated crystallization pattern. The H3 fraction of S-0.2 appears to form a mixed α-phase quantitatively dominated by PPP that demixes during polymorphic transition into β. H3 fractions with predominantly SSS (S-0.4, S-0.8) already show an immiscibility in the α-phase.

3.2. Time-Resolved Small- and Wide-Angle X-ray Scattering. The isothermal crystallization behavior of the H3 + H2U blends with different H3/H2U ratios (0.2, 0.4, and 0.8) for two H3 sources (FHRO vs POSt) was studied via time-resolved SAXS. The evolution of crystalline phases during cooling at varying cooling rates (1, 5, and 10 °C min^{-1}) and during the 30 min isothermal holding time was followed. In this study, the *d*-spacing and (normalized) integrated intensity of the first-order reflection in the SAXS region were analyzed.

https://doi.org/10.1021/acs.cgd.4c01138
Cryst. Growth Des. 2024, 24, 9951−9964

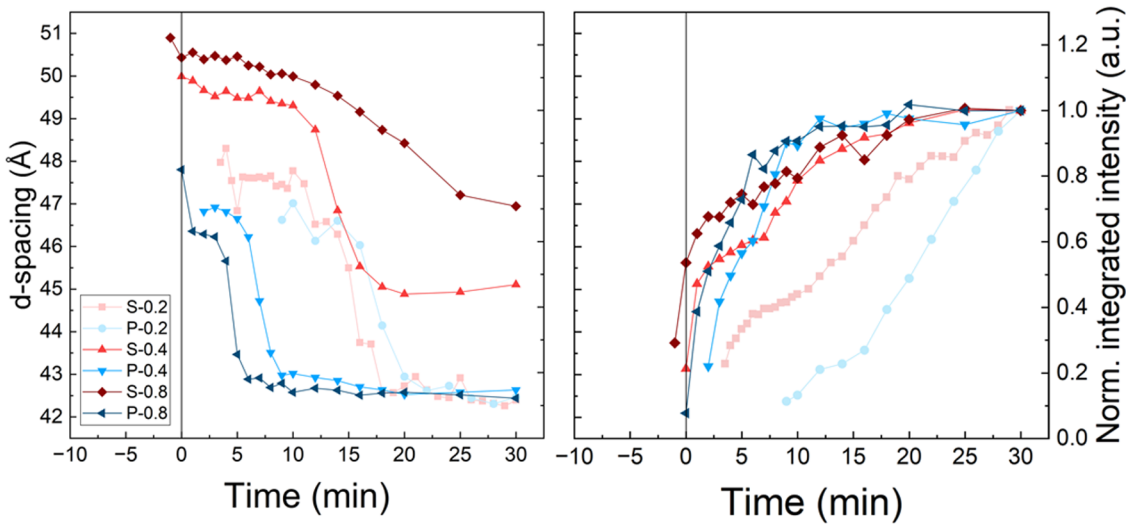

Figure 4. *d*-Spacing (left panel) and normalized integrated intensity (right panel) over isothermal time obtained after crystallization at 5 °C min^{-1} and an isothermal holding time for 30 min at 25 °C. H3/H2U ratio of 0.2 (squares), 0.4 (circles), and 0.8 (triangles). Sample with FHRO as H3 source in red and samples with POSt as H3 source in blue.

The *d*-spacing representing the lamellar stacking is a function of the number of carbon atoms and polymorphic form present. Tables S1 and S2 in the Supporting information summarizes the long and short spacings of selected triglycerides as reported in the literature.

The *d*-spacing derived in this study needs to be interpreted, combining two different pieces of information: (i) the TAGs present and (ii) the polymorphic form as derived from the WAXS region. This way, we related the composition to the different crystalline phases.

Figure 3 gives the SAXS and WAXS patterns for S-0.8 and P-0.8 crystallized at 5 °C min^{-1}. Table 4 summarizes the long and short spacings of the selected patterns.

3.2.1. Effect of the H3/H2U Ratio. Figure 4 gives the *d*-spacing and normalized integrated intensity (reference being the integrated intensity after 30 min, i.e., the end of the isothermal phase) over time for the blends cooled down at a rate of 5 °C min^{-1}. The start of the isothermal time was set to 0 min. The first-order reflection was used to determine the value of the *d*-spacing (i.e., lamellar stacking) and normalized integrated intensity (i.e., the degree of crystallinity). The WAXS pattern shows at least two phases coexisting; nevertheless, the SAXS region does not give detailed information of the stacking of the respective phases; see Figure 3. Hence, the *d*-spacing discussed in this article is an average value representing an average lamellar stacking per time frame analyzed. A similar note is necessary on the normalized intensity. This was calculated in the first-order region of q from 0.6 to 1.8 nm^{-1} and normalized against the value at the end of the isothermal holding phase, i.e., 30 min. For reference, the integrated intensities recorded after cooling at 5 °C/min and 30 min under isothermal conditions are given in Table 5. Multiple phases present at the same time were not taken into account. Hence, the values reported are only qualitative indicators for the degree of crystallinity and do not allow for a quantitative view of the amount of phases present at the same time.

The FHRO-PO blends show consistently higher *d*-spacings than POSt-based blends. The P-based blends show a stepwise evolution of the *d*-spacing, whereas when FHRO is added to PO, the picture is less clear. The changes in the *d*-spacing can be interpreted in two ways: either a polymorphic transition takes place or the composition changes, or both are occurring simultaneously.

Table 5. Integrated Intensities Determined from q = 0.6 to 1.8 nm^{-1} Given at the End of the Isothermal Holding Time (30 min) After Cooling at 5 °C/min

sample	integrated intensity (a.u.)
P-0.2	216.13
S-0.2	161.41
P-0.4	263.05
S-0.4	309.07
P-0.8	377.52
S-0.8	348.28

The integrated intensity of the P-0.2 and S-0.2 samples, H3 in both cases predominantly given by PPP, indicates that the crystallization was not completed after 30 min isothermal crystallization. A similar observation was made when the blends were cooled at 10 and 1 °C min^{-1} (data not shown). Both blends show a two-step evolution of the *d*-spacing. Initially, the *d*-spacing is around 48 and 46 Å for S-0.2 and P-0.2, respectively. For P-0.2 this corresponds well to the *d*-spacing of PPP in the α-polymorph being 45.6 Å.[29] The *d*-spacing of the S-0.2 sample is somewhat higher due to the presence of SSS which corresponds to a value of 50.6 Å.[29] Similar *d*-spacings were recorded by Foubert et al.[30] for 2% FHRO in PO, which is a comparable blend to this study's S-0.2. At higher H3/H2U ratios, the *d*-spacings of the S-samples (S-0.4 and S-0.8) are greater than those for the P-samples, indicating the dominant role of the H3 triglycerides. POSt-PO (0.4 and 0.8) blends undergo polymorphic changes much faster. The subtle changes in *d*-spacing in the S-based samples also hint at polymorphic transitions and changes in the composition simultaneously. However, the lab-scale SAXS/WAXS instrument used did not allow for resolving the underlying peaks. The kinetic differences between the P and S-based blends are more reflected in the integrated intensities.

3.2.2. Effect of the Cooling Rate. To study the possibility of kinetically triggered phase segregation during crystallization,

https://doi.org/10.1021/acs.cgd.4c01138
Cryst. Growth Des. 2024, 24, 9951−9964

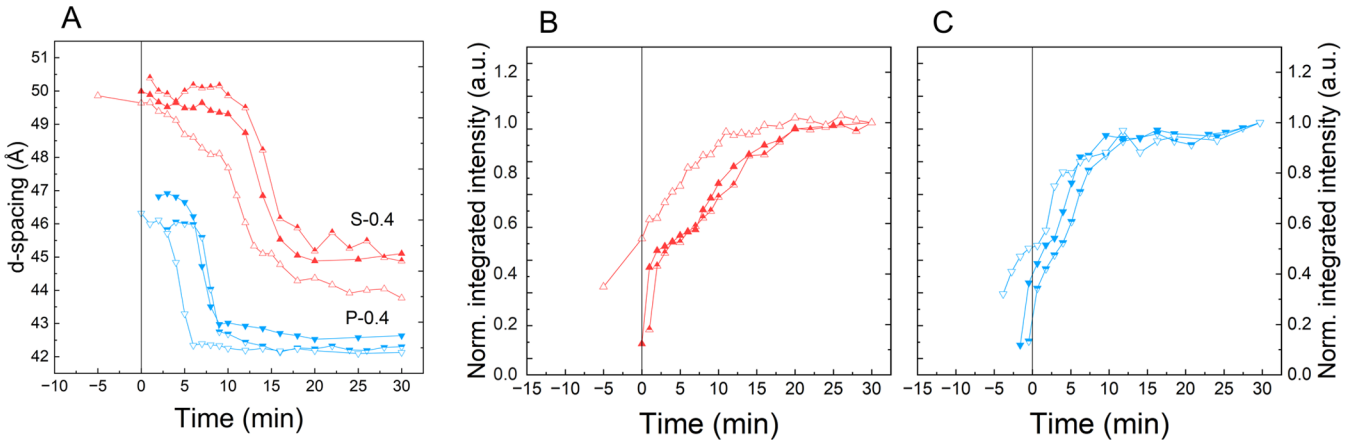

Figure 5. (A) *d*-spacing over isothermal time for S-0.4 (red) and P-0.4 (blue) at different cooling rates: 1 °C min^{-1} (hollow symbols), 5 °C min^{-1} (solid symbols), and 10 °C min^{-1} (half up symbols). (B) Normalized integrated intensities for S-0.4. (C) Normalized integrated intensities for P-0.4.

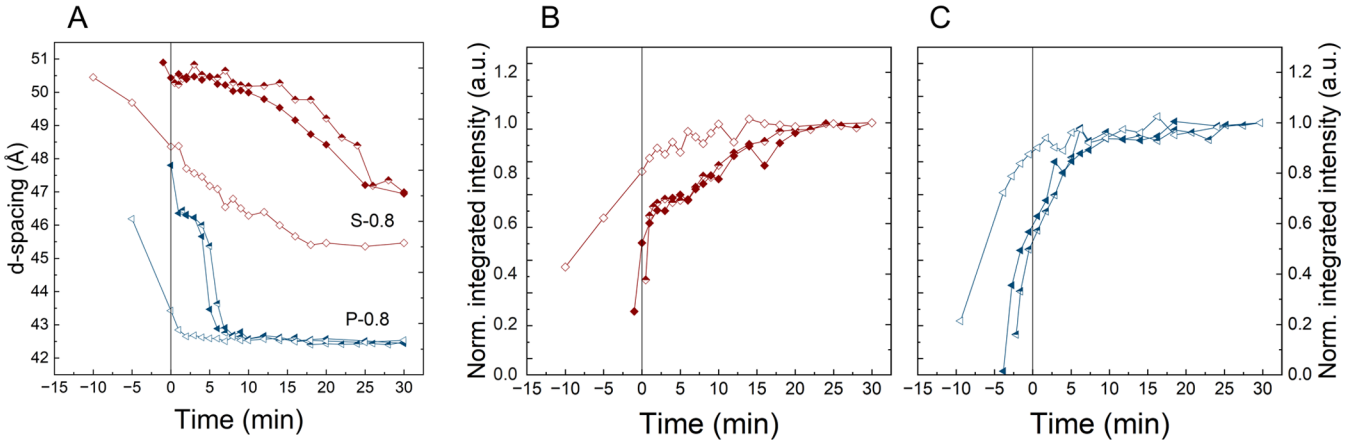

Figure 6. (A) *d*-spacing over isothermal time for S-0.8 (red) and P-0.8 (blue) at different cooling rates: 1 °C min^{-1} (hollow symbols), 5 °C min^{-1} (solid symbols), and 10 °C min^{-1} (half up symbols). (B) Normalized integrated intensities for S-0.8. (C) Normalized integrated intensities for P-0.8.

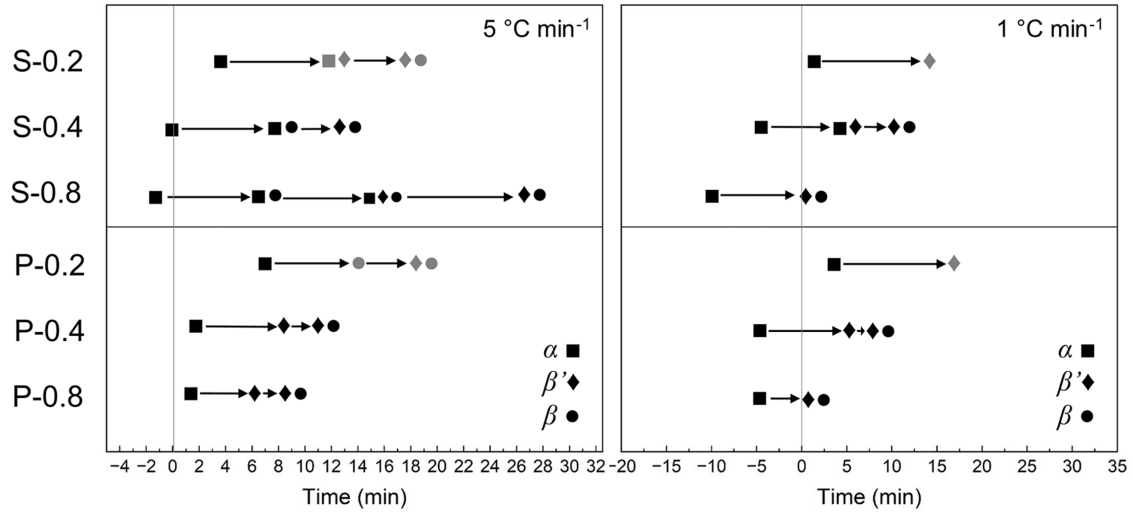

Figure 7. Qualitative representation of polymorphs identified in the WAXS region per time frame after cooling at 5 and 1 °C min^{-1}. Signal intensity was the highest for blends S-0.8 and P-0.8 and lowest for blends P-0.2 and S-0.2, making the polymorph identification for the latter less secure. Hence, less secure phase allocations are given as gray symbols.

three different cooling rates (1, 5, and 10 °C min^{-1}) were applied prior to isothermal holding at 25 °C. Figures 5 and 6 give the related *d*-spacings and normalized integrated intensities over time for blends P-0.4/S-0.4 and P-0.8/S-0.8,

https://doi.org/10.1021/acs.cgd.4c01138
Cryst. Growth Des. 2024, 24, 9951−9964

respectively. Again, the start of the isothermal time was set to be zero min.

All blends show a single-step decrease in *d*-spacing with the exception of S-0.8. In this case, the transition appears rather continuous. The effect of the cooling rate variation is negligible for P-blends. Neither the *d*-spacings nor the intensities vary greatly. It is, however, noteworthy that the graph might suggest that the lowest cooling rate results in faster crystallization. This is not the case. All time axes are normalized to the beginning of the isothermal period. The isothermal temperature is, by design, lower than the saturation temperature for the respective blend. This intrinsically causes blends subjected to the lowest cooling rates to be the longest under supersaturation conditions prior to the isothermal period.

The S-blends are more affected by the different cooling rates. While the initial *d*-spacing is identical for all cooling rates, the final *d*-spacing is reduced by about 1 and 2 Å for S-0.4 and S-0.8, see Figures 5 and 6, respectively. Also, the transition from the initial recorded *d*-spacing takes place more slowly than that when applying higher cooling rates for S-0.8. Cooling the sample from 70 down to 25 °C at 1 °C min^{-1} takes as long as cooling at 5 °C min^{-1} plus an additional 30 min isothermal crystallization time. Yet, the *d*-spacing at 0 min (start of the isothermal period) is larger when crystallized at 1 °C min^{-1} than at other cooling rates. This is possibly due to SSS crystallizing separately, whereas it is more inclined to cocrystallize, when higher cooling rates are applied. After 30 min of isothermal crystallization samples S-0.8 and S-0.4 yield similar *d*-spacings close to the values reported for SSS in the β' and β phase.[29]

A less steep decrease in *d*-spacing is observed in S-0.4 and S-0.8 contrary to that in the P-based counterparts. S-0.4 shows three levels of *d*-spacing: 49.5 Å during the cooling phase, 48 Å after 5 min of isothermal hold, and 44 Å after 20 min isothermal hold. This multiple-step decrease corresponds well with the evolution of integrated intensities. No difference in *d*-spacing evolution over time at different cooling rates can be reported for the blends with an H3/H2U ratio of 0.2 (data not shown).

3.2.3. Effect of the H3 Molecular Makeup on the Polymorphic Pathway. A qualitative evolution of the different polymorphs identified via the WAXS region and their occurrence over time is given in Figure 7. The data obtained at 10 °C min^{-1} do not differ greatly from those obtained at 5 °C min^{-1} and, hence, are not shown.

When crystallized at 1 °C min^{-1}, the polymorphic pathways of blends of different H3 (FHRO vs POSt) sources only differ marginally. For both, FHRO and POSt added to PO, the α polymorph forms during cooling. After reaching the crystallization temperature, the blends undergo a transition into β' phase, either coexisting briefly with the α phase as for S-0.4 or as the sole intermediate state. In any case, the intermediate stage is only observed briefly. All blends show coexisting β' and β phases in the end except for P-0.2 and S-0.2. This final state is reached faster with increasing H3/H2U ratio.

The final state of coexisting β' and β phases was found for all blends when crystallized at a scan rate of 5 °C min^{-1}. However, differences in the intermediate stage become apparent when comparing FHRO and POSt added to PO. Starting from the α polymorph, the POSt-PO blends transition into β' polymorphs. This intermediate state is followed by coexistence of β' and β polymorphs. In contrast, the intermediate state of the FHRO-PO blends is characterized by coexistence of the original α phase with a β polymorph. Conversion via the coexistence of three polymorphs, α, β', and β, leads again to the formation of coexisting β' and β polymorphs. The observed coexistence of α and β phases before a β' phase indicates a separate crystallization of an SSS-rich α−phase transitioning into its presumably most stable polymorphic form (β) before mixed phases containing H2U triglycerides crystallize.

In summary, all blends exhibit coexisting β' and β phases after 30 min isothermal crystallization. Also, the α polymorph occurs initially independent of the blend and cooling rate. The main differences found are coexisting phases at intermediate stages. This appears to be dependent on whether the H3 fraction is P- or S-based and on the H3 dosage.

Combining the information obtained about the polymorphic states and lamellar stacking allows for the following interpretation. In the FHRO-PO blends (H3 fraction consisting of SSS and PPP, with SSS dominating in S-0.4 and S-0.8), the SSS-rich α phase undergoes a transition directly to the β phase as we did observe for FHRO in previous research.[20] In this case, however, the transition is slower due to the presence of H2U triglycerides. One cannot ignore the diglycerides and other minor components in PO and their effects on the crystallization.[31] Diglycerides affect the crystallization via heterogeneous nucleation and surface poisoning during crystal growth.[21,32] Structural dissimilarities in the TAG fraction affect the polymorphic transition. In mixtures of PPP and PSP, the structural dissimilarities altered PPP's polymorphic pathway in the way that a β' phase formed which was not observed in experiments with exclusively PPP.[33] Further, it was reported that the polymorphic transition of monoacid triglycerides can be accelerated in the presence of a fraction of similar crystallization temperature as reported for LaLaLa and the molecular compound $MC_{SOS/OSO}$[34] In this study, similar dissolution temperatures of the H3 and H2U fraction can be assumed due to their different concentrations, H3 lower than H2U. However, as Figure 7 reveals this sequence of polymorphs appearing with intermediate coexistence of α and β phases does not appear at a lower cooling rate.

Different from SSS, PPP is most likely to cocrystallize with PPO/POP. PPP/POP and PPP/PPO mixtures are immiscible in metastable and stable polymorphic forms. PPP can undergo a transition into the intermediate β' form at POP concentrations above 50%[35] similar to the effects reported for PPP and PSP.[33] Also, similar behavior can be derived from recent data on PPP and the molecular compound $MC_{POP/PPO}$.[14] Furthermore, it is reported that β-PPP crystals can accommodate about 40−50% of POP.[35] The *d*-spacing data throughout the study suggest that no 3L-polymorphs form, which is a characteristic of POP in the β phase.[36] The coexistence of β' and β phases allows us to conclude that in the palmitic-based blends, the H3 and H2U components cocrystallize partly to form a medium-melting mixed crystalline phase rich in H2U and a high-melting phase rich in H3 with limited inclusion of H2U triglycerides.

The blends S-0.4 and S-0.8 can be regarded as a ternary system consisting of SSS, PPP, and POP. Here, the components compete kinetically to form different mixed crystals. The evolution of *d*-spacings and its dependence on the H3 dosage in the S-samples clearly reveals coexisting crystalline phases of different compositions as suggested in the polymorphic pathways.

https://doi.org/10.1021/acs.cgd.4c01138
Cryst. Growth Des. 2024, 24, 9951−9964

Nevertheless, it remains difficult to determine the compositions of the different crystalline phases. SAXS experiments with a higher resolution could be useful for deconvolution of potentially overlapping reflections.

3.3. Isothermal Crystallization via DSC and Oscillatory Shear Rheology. The isothermal crystallization was studied by DSC and oscillatory shear experiments. Figure 8 gives the time-resolved DSC signal of both H3 and H2U systems. The DSC signal for RP without any hardstock added is given for reference.

For the POSt-PO system, the time-resolved DSC signal shows two exothermic events. This is in line with Figure 4—two-step evolution in *d*-spacing. Also, the first crystallization event occurs earlier with increasing H3/H2U ratios. S-0.2 shows very similar behavior. The S-blends with a higher H3/H2U system show three crystallization events. This is again in line with the data shown in Figure 4—slow restructuring. The fact that H2U triglycerides, beyond crystallizing themselves, significantly alter the crystallization of the H3 fraction is further documented considering the data for H3(S-0.4) and H3(S-0.8), see Figure 2.

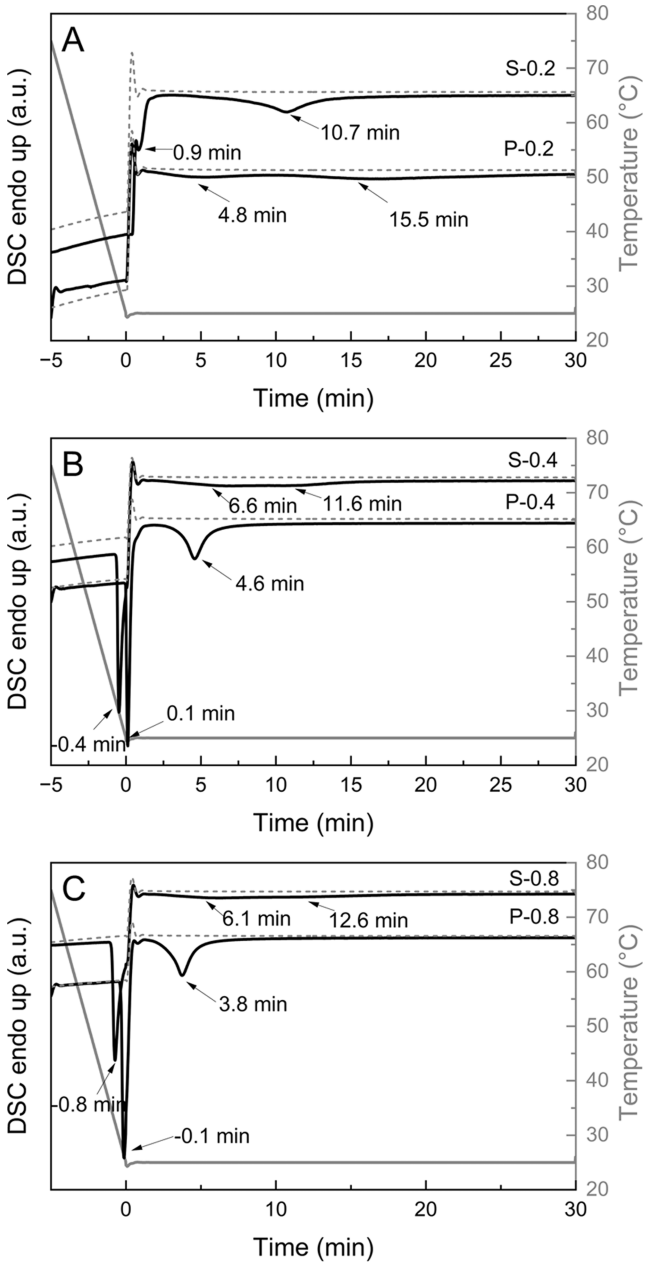

Figure 8. DSC signal over time obtained during cooling at a rate of 10 °C min^{-1} and during the isothermal time, exothermic events down. Time zero was set to the starting point of the isothermal phase. Time of the exothermal event was as indicated. The DSC signal obtained for rapeseed oil without any hardstock added is given as a gray-dashed line for reference.

Overall, comparing the time-resolved DSC signals to the ones obtained for the H3 system reveals that the addition of H2U to the FHRO-PO blends results in a delay in the crystallization of the higher-melting components. This is in good agreement with literature data on the crystallization of mixtures containing H3 and H2U triglycerides, i.e., saturated and monounsaturated triglycerides.[37,38]

The microstructural development during isothermal crystallization of the H3 + H2U systems was studied by using oscillatory shear rheology. Previous studies claim that rheological methods are able to record polymorphic transition besides multiple-step crystallization.[5,15] The same temperature−time profile was applied as in the calorimetric study. Figure 9 gives the evolution of the complex modulus, |*G**|, over time.

The FHRO-PO systems show a two-step evolution of |*G**| over time, characterized by a rapid increase in |*G**|, followed by a plateau-like region and a second sharp increase in |*G**| until the signal flattens to a constant value. With increasing ratio of H3/H2U the plateau-like region is recorded earlier and at higher |*G**| values. The first sharp increase of |*G**| in the oscillatory shear experiments can be compared to the first crystallization events visible in the time-resolved DSC signal (Figure 8). At this point, it must be noted that a comparison of the exact time scales is limited due to the different thermal lags of the measurement techniques. Still, the first crystallization event matches the sudden increase in |*G**|, and the second event aligns with reaching a constant |*G**| value. However, the third crystallization event found for S-0.4 and S-0.8 in Figure 8 was not detected when the complex modulus. This is either because the rheological effects of the two events being very fast overlap or the second crystallization event does not cause a detectable effect due to the nature of the crystallization. Heterogeneously nucleated crystallization events might only cause the compaction of spherulites without changing their hydrodynamic radius.

The POSt-PO systems undergo a similar |*G**| evolution. In line with the DSC data, the first crystallization event is monitored at shorter times for the S-based systems. Except for P-0.2 the data also confirm that the second crystallization event occurs earlier in P-based systems. The fact that S-0.2 also contains more PPP than SSS might be the root cause of this exceptional effect of the P-based H2U TAGs.

The results contradict previous literature that claims that oscillatory shear experiments allow monitoring of polymorphic crystallization.[5,15] In this study, the composition of the blends resulted in a different signal, and additional events recorded by DSC do not match the evolution of the complex modulus. Rheological tests are sensitive to the microstructure development[5,6,17] which at best could be a derivative of polymorphic transitions. The polymorphic transition may affect the microstructure by inducing changes in the morphology of the crystal network and the crystal size distribution. This is also in line with the results from a previous study of this lab, where

https://doi.org/10.1021/acs.cgd.4c01138
Cryst. Growth Des. 2024, 24, 9951−9964

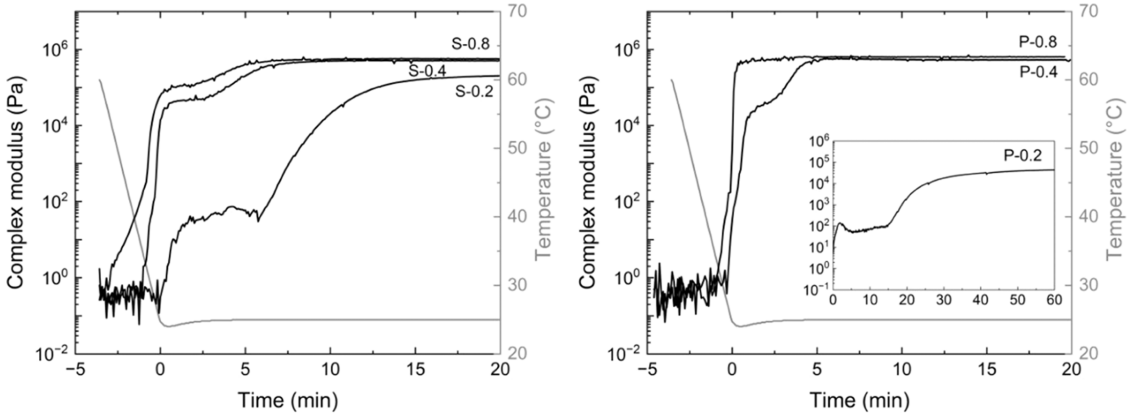

Figure 9. Complex modulus over time by applying a cooling rate of 10 °C min^{-1}. Time zero set to the starting point of the isothermal phase. Left: FHRO-PO, right: POSt-PO. Note, P-0.2 displayed in a zoom over 60 min under isothermal conditions.

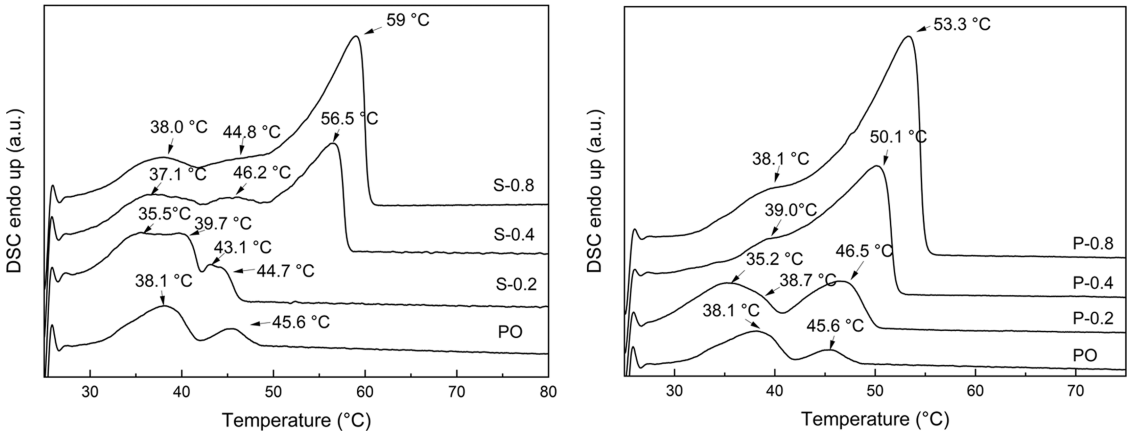

Figure 10. Left: DSC melting curves of the FHRO-PO system; PO, right: DSC melting curves of the Pos-PO system, PO. Heating rate 2 °C min^{-1}. Cooling rate 10 °C min^{-1}. Melting peaks as identified.

DSC and time-resolved SAXS/WAXS studies showed two-step crystallization clearly attributable to polymorphic transitions that were not recorded as changes in the complex modulus.

3.4. Calorimetric Study of the H3 + H2U Systems. The crystallization pathways can be documented in the melting profiles. The melting behavior of H3 + H2U blends with different H3/H2U ratios (0.2, 0.4, and 0.8) for two H3 sources (FHRO vs POSt) is shown in Figure 10. On the left and the right the respective melting curves for the FHRO system and POSt system are shown. For reference, the melting profile of exclusively PO (without the H3 source) subjected to the same process (cooled at 10 °C min^{-1} to 25 °C and held for 30 min) is given as well.

The reference (PO) shows two broad melting peaks at 38.1 and 45.6 °C. The addition of H3 (POSt) in the POSt-PO system (right) causes an increase in both signal strength and peak temperature of the higher melting peak. On mixing PO and FHRO the H3 fraction becomes more mixed, mainly PPP and SSS. The blend with the lowest H3/H2U ratio (S-0.2) and an SSS:PPP ratio of 21:79 shows two overlapping high-melting peaks at 43.1 and 44.7 °C. These temperatures are lower than observed for straight PO (45.6 °C) and the respective H3 fraction (H3(S-0.2)) (49.5 °C), see Figure 1. This indicates that the H2U triglycerides influence the SSS and PPP crystallization significantly more strongly than just serving as a solvent. They rather change the crystallization through selective cocrystallization. With higher concentrations of FHRO and hence higher ratios of H3/H2U and SSS to PPP (S-0.4 and S-0.8) the melting pattern evolve toward a superimposed melting diagrams of PO and of H3(S-0.8) in Figure 1. Comparing the P- and S-based systems, it becomes apparent that the peaks around 38 °C originate from PO, and the intermediate peak in S-based systems, around 45 °C, is related to a PPP-rich solid phase. It should be noted that the PPP level in these systems is slightly lower than in pure PO which renders the increased temperatures a consequence of limited mixed crystal formation.

The highest peak temperatures in S systems are higher than those in P systems once SSS is the dominant TAG in H3 by mass fraction. These temperatures correspond quite well with the data gathered for H3 systems (Figure 1).

Overall, the multiple melting events documented in the melting profile for the S-based samples are in good agreement with the complex polymorphic pathways and slow restructuring documented in the time-resolved X-ray studies. While in the end only two polymorphs were found to be present, the *d*-spacing hinted toward a more complex picture. Similarly, the two-step melting of the POSt-PO samples is in good agreement with the coexisting β' and β phases and the comparably simple two-step evolution of *d*-spacing.

3.5. Effect of the TAG Melting Group on the Polymorphic Transition. In this study, the crystallization is dominated by H3 rather than H2U triglycerides. The POSt-PO mixture gives insights into the polymorphic pathway of H3

https://doi.org/10.1021/acs.cgd.4c01138
Cryst. Growth Des. 2024, 24, 9951−9964

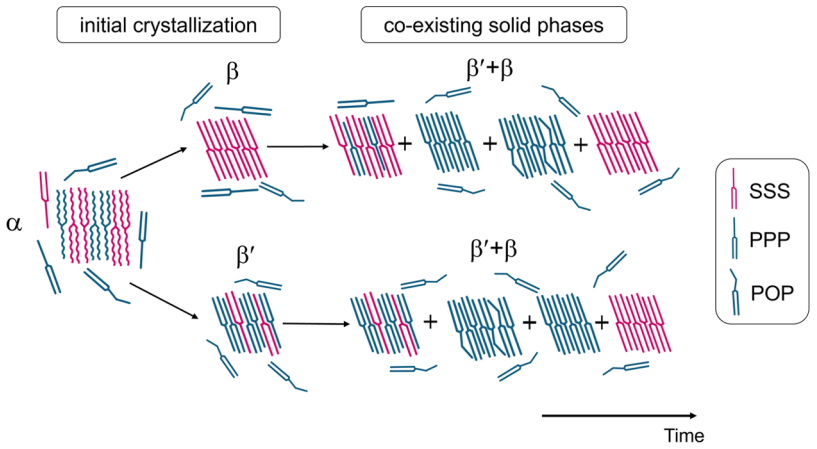

Figure 11. Schematic representation of selective cocrystallization occurring in a blend of two trisaturated triglycerides and a monounsaturated triglyceride of different molecular compositions. The monounsaturated triglycerides influence the crystallization of trisaturated triglycerides through selective cocrystallization. The samples S-0.4 and S-0.8 (top) rich in SSS first crystallize into a solid fraction of exclusively SSS, further cocrystallize in metastable forms with PPP, which also cocrystallizes with POP. Sample S-0.2 (bottom) shows a mixed crystal of PPP and SSS, which separates during melting into an SSS and PPP-rich crystals as well as into a mixed crystalline phase of PPP and POP.

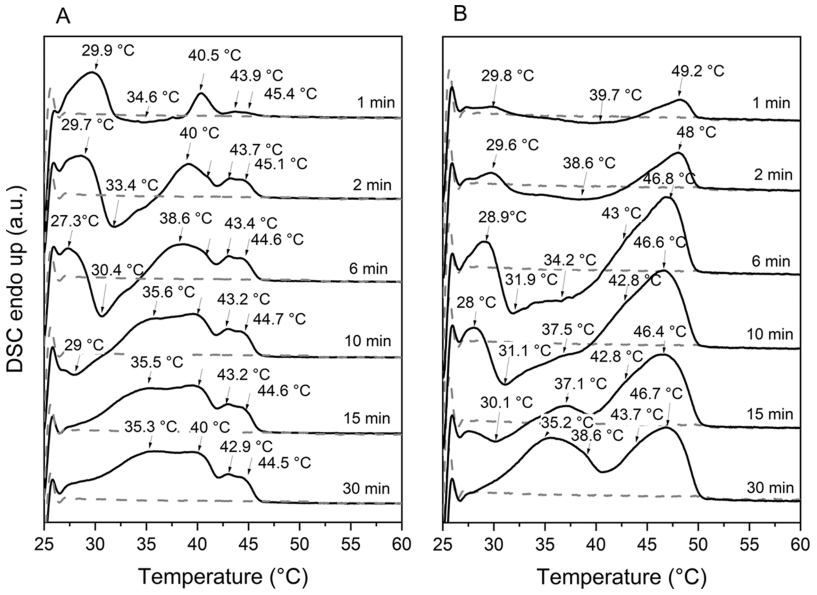

Figure 12. DSC melting curves obtained at 2 °C min^{-1} of (A) S-0.2 and (B) P-0.2 after crystallizing by cooling at 10 °C min^{-1} for different holding times at 25 °C. Identified endothermic and exothermic peaks as indicated. Rapeseed oil without any crystallizing material added is given as dashed lines for reference.

triglycerides in the presence of H2U triglycerides of comparable molecular makeup, e.g., PPP and POP/PPO, whereas the FHRO-PO mixtures consist of triglycerides of substantial structural dissimilarities, e.g., SSS and POP. In the POSt-PO system, the increase in H3 dosage did not alter the recorded *d*-spacings at the start of the crystallization nor the final *d*-spacing but facilitated the crystallization. The higher the H3/H2U ratio, the faster the crystallization, displaying only minimal differences in the polymorphic pathways. In contrast, the polymorphic pathways in the FHRO-PO blends did change with an increasing H3/H2U ratio. Note, the H3 fraction is a mixture and consists of mostly SSS from FHRO and PPP from PO. In these blends, an increase in the H3/H2U ratio resulted in multiple coexisting crystalline phases and an overall longer persisting α phase (Figure 7). The lamellar spacing (Figure 4) increased with the H3/H2U ratio indicating a dominant role of SSS. Hence, the prolonged existence of the α phase is attributed to SSS. Experimental studies on the binary mixture of SSS and PPP suggest demixing in the α phase exceeding 30% SSS in the mixture and a cooling rate below 20 °C min^{-1}[27,28] which is in line with the experimental conditions of this study. Comparing the results from the experiments concerning only the H3 fraction of the FHRO-PO blends to the results of the FHRO-PO blends shows that the addition of H2U triglycerides slows down the crystallization process of the H3 fraction and actively inhibits the fast transition into β via selective cocrystallization. After 30 min holding at 25 °C the β' and β polymorphic forms coexist (Figure 7). It is noteworthy that the identical polymorphic state was reached for almost all samples except for P-0.2 and d S-0.2, and this, despite the variation in the *d*-spacing evolution during the isothermal holding time. A proposed pathway illustrating the concept of selective cocrystallization is shown in Figure 11. Depending on the driving force per TAG, the respective TAG is either

https://doi.org/10.1021/acs.cgd.4c01138
Cryst. Growth Des. 2024, 24, 9951−9964

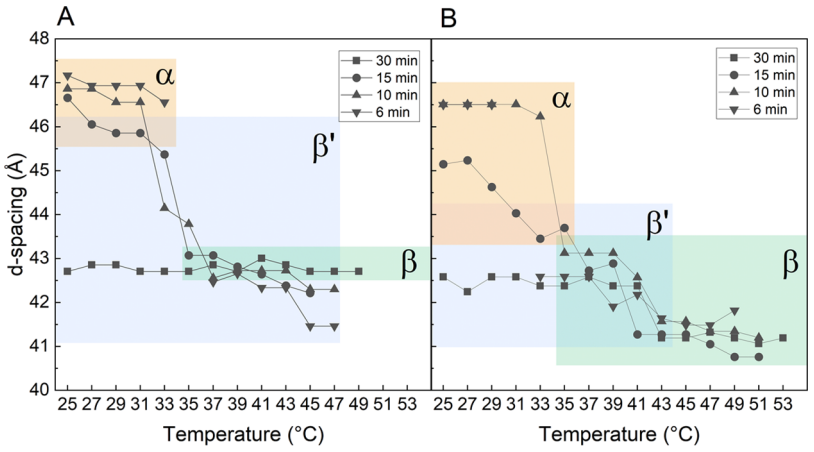

Figure 13. Evolution of *d*-spacing in the SAXS region recorded during melting at 2 °C/min for (A) S-0.2 and (B) P-0.2 after increasing isothermal holding times: 6 min (downward facing triangles), 10 min (upward facing triangles), 15 min (circles), and 30 min (squares). Polymorphs as identified from WAXS and color coded: α (orange), β' (blue), β (green). Overlapping regions indicate coexisting crystalline phases assigned to the same *d*-spacing.

inclined to form a mixed crystal, i.e., cocrystallize, or undergo a phase transition on its own. This means that a TAG is not exclusively found in one phase or the other (mixed or separate) but can be distributed in multiple crystalline phases of different polymorphic forms and compositions.

3.6. Mixed Crystal Formation of H3 Triglycerides in the Presence of H2U Triglycerides. The samples S-0.2 and P-0.2 with the lowest concentration of added H3, either FHRO or POSt, showed little difference in the *d*-spacings and polymorphic pathways. However, the melting profiles especially in their high-melting region differed. For S-0.2, a double high-melting peak indicated the separate melting of two H3-rich β-phases, one rich in SSS and the other rich in PPP (Figure 10). Data on the H3 fraction in S-0.2 in the absence of H2U (Figure 1) revealed only one melting peak. However, at the given composition (7.6% PPP and 2% SSS), the respective dissolution temperatures of SSS and PPP are very similar such that both fractions dissolve around 50 °C. Neither the melting profiles nor the SAXS/WAXS pattern allows to distinguish mixed or separate α-phases.

To investigate the formation of presumed mixed crystal(s) during early crystallization, DSC melting curves were obtained after subjecting S-0.2 to various isothermal holding times and melting subsequently at 2 °C min^{-1} (stop-and-return). The same experiments were performed with P-0.2 for comparison; both are displayed in Figure 12.

In Figure 12A a low-melting peak at 29.9 °C can be seen, followed by a recrystallization peak. Later, a second melting peak at 40.5 °C occurs along with a doublet peak for the FHRO in the PO sample—two merged high-melting peaks. It becomes apparent, that the doublet peak is recorded after crystallizing S-0.2 for only 1 min and remains constant when the holding time exceeds 6 min, indicating no further changes of composition. P-0.2 also shows a low-melting peak at 29.8 °C (Figure 12B) similar to that of S-0.2. After a recrystallization, one single high-melting peak is observed at 49.2 °C. Its temperature decreases with increasing isothermal holding time. The fact that more solid material dissolves at a lower temperature indicates a continuous change of the composition of the high-melting crystal in the first 6 min. At longer crystallization time this peak remains unchanged and an additional solid phase appears as a shoulder at 43 °C.

The low-temperature peak in both systems is assigned to the α-phase. However, looking carefully at the evolution, one finds that the polymorphic transition clearly coincides with the peak appearance. The longer the isothermal holding times, the more the transition has proceeded prior to heating. This moves the peak to lower temperatures and lower enthalpies. Anyhow initially the enthalpy increases due to ongoing crystallization of the α-phase.

To verify the polymorphic forms and to understand the lamellar stacking and alkyl-chain packing, SAXS/WAXS analyses were performed, following the same temperature−time profile, i.e., allowing the sample to crystallize for different times, and the subsequent melting was evaluated. The evolution of *d*-spacing during the melting including the polymorph identification is displayed in Figure 13.

When S-0.2 was crystallized for only 6 min, the initial *d*-spacing at the start of the melting was 47 Å (Figure 13A). It is important to note here, that even though the same temperature−time profiles were applied in the DSC and SAXS/WAXS experiments, the SAXS/WAXS data lag behind due to different thermal lag. With more time to crystallize, 10 and 15 min, the initial α phase, identified by WAXS—the *d*-spacings decreases to 46.5 and 46 Å, respectively. This indicates either a different packing and/or composition. After 30 min, the initial *d*-spacing was 43 Å and identified to relate to the β'-polymorph. This corresponds, despite minute temperature shifts, very well to the low-melting peaks recorded via DSC. In contrast, the initial *d*-spacing of P-0.2 is 46.5 Å (α-phase) and decreases only after 15 min. The drop to 45.2 Å is more drastic than that for S-0.2.

While S-0.2 tends to develop the β' polymorph (two-step evolution in *d*-spacing), P-0.2 assumes predominantly the β polymorph (three-step evolution of *d*-spacing). The initial *d*-spacings of S-0.2 are slightly larger than those of P-0.2. This indicates the influence of a small amount of SSS in PPP-dominated crystal structures (S-0.2). In combination with the DSC signals obtained (Figure 12) it is evident that the FHRO fraction in S-0.2 affects early-stage crystallization. However, given the data at hand, it remains difficult to explore mixed crystal formation in the α phase including a definite composition of the phase. Yet, the binary phase behavior known for SSS/PPP and the experimental conditions allow a mixed crystal formation in the α-phase. A mixed α-phase

https://doi.org/10.1021/acs.cgd.4c01138
Cryst. Growth Des. 2024, 24, 9951−9964

subsequently segregates in the presence of H2U triglycerides into two phases. This reasoning is in line with the doublet peak observed in the thermograms.

4. CONCLUSIONS

This contribution is the second part of a series examining the crystallization pathways, particularly polymorphic transitions, as a function of the TAG composition in complex fat blends. This research mainly discusses the effect of H2U triglycerides on the polymorphic crystallization of H3 triglycerides. The findings are compared to the presumed mixed crystal formation in mixtures of H3 and H2M triglycerides and a system containing only H3 triglycerides—addressed in a previous study of our lab.[20] The effect of composition on polymorphic crystallization in H3 + H2U blends was investigated by varying the H3/H2U ratio. Variation included different H3 sources added to PO (FHRO vs POSt), processing conditions, cooling rate, and holding times. DSC, time-resolved SAXS/WAXS, and oscillatory shear experiments were used to unravel the melting behavior and nano- and microstructural development.

In line with the previous study on H3 and H3 + H2M triglycerides,[20] the blends showed a multiple-step crystallization process generally facilitated by higher H3 levels. Differences due to the H3 source were found. The POSt-PO blends showed a two-step crystallization process, clearly manifested in the two-step decrease in d-spacing, the two crystallization events recorded via DSC, and the two-step increase in the complex modulus. WAXS data revealed the blends crystallized into the α-phase, and subsequently underwent a phase transition into β' phase, and further into coexisting β and β' phases. These remained coexisting during the 30 min of isothermal crystallization. The FHRO-PO blends showed a more complex behavior, e.g., three exothermic events shown in DSC and a slow decrease of d-spacings. Accompanying WAXS data revealed multiple coexisting polymorphic forms and an α phase with a prolonged existence compared to the palmitic-based blends was observed. The stearic-based triglycerides underwent a polymorphic transition from α into β form before a β' phase could be detected, indicating independent crystallization events altogether.

Overall, the FHRO-PO blends crystallize faster than their POSt-PO counterparts, but the crystal structuring takes longer, as revealed by SAXS/WAXS. Yet, this restructuring (evolution of d-spacing) was not captured in the oscillatory shear experiments.

In general, palmitic-based triglycerides as in POSt form mixed crystals in parts, but once the H3 content exceeds a critical value, the crystallization pathway is dominated by the transition of PPP into the most stable polymorphic β form. Further, the results suggest that stearic-based high-melting triglycerides as in FHRO do not tend to form prevailing mixed crystals with PO components during the crystallization process. Even at low FHRO levels as in S-0.2, the presence of H2U triglycerides caused phase segregation.

By combining the data gathered from DSC and SAXS/WAXS it was possible to capture the polymorphic pathways amid mixed crystal formation in complex blends and link this to the melting behavior. Compared to earlier studies on palm oil, this work deliberately covered crystallization at an elevated temperature to ensure that only the TAG groups targeted in the experimental design were crystallizing. The data gathered here are nonetheless instrumental for the interpretation of palm oil-based blends crystallized at lower temperatures. Extending the study by variation of the temperature is certainly beneficial but introduces significant complexity by the presence of additional mixed solid phases due to the expected cocrystallization of HU2 TAGs.

■ ASSOCIATED CONTENT

Supporting Information

The Supporting Information is available free of charge at https://pubs.acs.org/doi/10.1021/acs.cgd.4c01138.

Details on the SAXS/WAXS data treatment including the subtraction of the liquid fraction, the analysis of the first order peak, and indexing of the diffraction pattern (2L-stacking); and summary of literature data on long and short spacings of pure triglycerides (PDF)

■ AUTHOR INFORMATION

Corresponding Author

Julia Seilert − *Department of Food Process Engineering, Technische Universität Berlin, Berlin 10623, Germany;* orcid.org/0000-0002-0149-7253; Email: julia.seilert@tu-berlin.de

Authors

Michael Rappolt − *School of Food Science and Nutrition, University of Leeds, Leeds LS2 9JT, U.K.;* orcid.org/0000-0001-9942-3035

Georg Dol − *Flora Food R&D B.V., Food Science Centre, 6708 WH Wageningen, The Netherlands*

Eckhard Flöter − *Department of Food Process Engineering, Technische Universität Berlin, Berlin 10623, Germany*

Complete contact information is available at: https://pubs.acs.org/10.1021/acs.cgd.4c01138

Notes

The authors declare no competing financial interest.

■ REFERENCES

(1) Sato, K.; Bayés-García, L.; Calvet, T.; Cuevas-Diarte, M. À.; Ueno, S. External factors affecting polymorphic crystallization of lipids. *Eur. J. Lipid Sci. Technol.* **2013**, *115* (11), 1224−1238.

(2) Marangoni, A. G.; Wesdorp, L. H. *Structure and Properties of Fat Crystal Networks*, 2nd ed.; CRC Press, 2013.

(3) Che Man, Y. B.; Haryati, T.; Ghazali, H. M.; Asbi, B. A. Composition and thermal profile of crude palm oil and its products. *J. Am. Oil Chem. Soc.* **1999**, *76* (2), 237−242.

(4) Smith, K. W. Crystallization of Palm Oil and Its Fractions. In *Crystallization Processes in Fats and Lipid Systems*; Garti, N., Ed.; Dekker, 2001; pp 357−380.

(5) De Graef, V.; Dewettinck, K.; Verbeken, D.; Foubert, I. Rheological behavior of crystallizing palm oil. *Eur. J. Lipid Sci. Technol.* **2006**, *108* (10), 864−870.

(6) Tangsanthatkun, J.; Wiking, L.; Sonwai, S.; Gregersen, S. B. Assessment of rheological methods to study crystallization of palm oil fractions. *J. Texture Stud.* **2021**, *52* (2), 169−176.

(7) Tarabukina, E.; Jego, F.; Haudin, J.-M.; Navard, P.; Peuvrel-Disdier, E. Effect of shear on the rheology and crystallization of palm oil. *J. Food Sci.* **2009**, *74* (8), E405−E416.

(8) Ng, W. L.; Oh, C. H. A kinetic study on isothermal crystallization of palm oil by solid fat content measurements. *J. Am. Oil Chem. Soc.* **1994**, *71* (10), 1135−1139.

(9) Mazzanti, G.; Marangoni, A. G.; Idziak, S. H. J. Modeling phase transitions during the crystallization of a multicomponent fat under shear. *Phys. Rev. E* **2005**, *71* (4), 041607.

(10) De Graef, V.; van Puyvelde, P.; Goderis, B.; Dewettinck, K. Influence of shear flow on polymorphic behavior and microstructural development during palm oil crystallization. *Eur. J. Lipid Sci. Technol.* **2009**, *111* (3), 290−302.
(11) Chen, C. W.; Lai, O. M.; Ghazali, H. M.; Chong, C. L. Isothermal crystallization kinetics of refined palm oil. *J. Am. Oil Chem. Soc.* **2002**, *79* (4), 403−410.
(12) Sainlaud, C.; Taché, O.; Testard, F.; Saiter, J.-M.; Bohin, M. C.; Coquerel, G. Impact of Cooling Profile on Refined Palm Oil Crystallization: Microscopic and Small and Wide-Angle X-Ray Scattering Investigations. *Eur. J. Lipid Sci. Technol.* **2022**, *124* (2), No. 2100045.
(13) West, R.; Rousseau, D. Tripalmitin-Driven Crystallization of Palm Oil: The Role of Shear and Dispersed Particles. *J. Am. Oil Chem. Soc.* **2020**, *97* (9), 989−999.
(14) Macridachis, J.; Bayés-García, L.; Calvet, T. Solid phase behavior of mixture systems based on tripalmitoyl glycerol and monounsaturated triacylglycerols forming a molecular compound. *Phys. Chem. Chem. Phys.* **2022**, *24* (6), 3749−3760. Published Online: Feb. 9, 2022.
(15) Breitschuh-Apostolakis, B.; Flöter, E. Solid immiscibility in milk fat fractions and methods to determine their occurrence. *Eur. J. Lipid Sci. Technol.* **2002**, *104*, 713−719.
(16) Mazzanti, G.; Marangoni, A. G.; Idziak, S. H. Synchrotron study on crystallization kinetics of milk fat under shear flow. *Food Res. Int.* **2009**, *42* (5−6), 682−694.
(17) Wiking, L.; Graef, V.; Rasmussen, M.; Dewettinck, K. Relations between crystallisation mechanisms and microstructure of milk fat. *Int. Dairy J.* **2009**, *19* (8), 424−430.
(18) Cisneros, A.; Mazzanti, G.; Campos, R.; Marangoni, A. G. Polymorphic Transformation in Mixtures of High- and Low-Melting Fractions of Milk Fat. *J. Agric. Food Chem.* **2006**, *54* (16), 6030−6033.
(19) van Aken, G. A.; Grotenhuis, E. T.; van Langevelde, A. J.; Schenk, H. Composition and Crystallization of Milk Fat Fractions. *J. Am. Oil Chem. Soc.* **1999**, *76* (11), 1323−1331.
(20) Seilert, J.; Rappolt, M.; Dol, G.; Flöter, E. Interplay of Polymorphic Transition and Mixed Crystal Formation in Model Fat Systems. *Cryst. Growth Des.* **2024**, *24* (3), 1146−1158.
(21) de Oliveira, I. F.; Grimaldi, R.; Gonçalves, L. A. G. Effect of diacylglycerols on crystallization of palm oil (Elaeis guineensis). *Eur. J. Lipid Sci. Technol.* **2014**, *116* (7), 904−909.
(22) Sato, K.; Kuroda, T. Kinetics of melt crystallization and transformation of tripalmitin polymorphs. *J. Am. Oil Chem. Soc.* **1987**, *64* (1), 124−127.
(23) Kellens, M.; Reynaers, H. Study of the Polymorphism of Saturated Monoacid Triglycerides I: Melting and Crystallization Behaviour of Tristearin. *Lipid/Fett* **1992**, *94* (3), 94−100.
(24) Bayés-García, L.; Macridachis, J.; Calvet, T.; Sato, K. In situ analyses of crystallization behavior of 1,2,3-tripalmitoyl glycerol under static and dynamic thermal conditions. *J. Therm. Anal. Calorim.* **2024**, *149*, 5215−5227.
(25) Lutton, E. S. Phase behavior of triglyceride mixtures involving primarily tristearin, 2-oleyldistearin, and triolein. *J. Am. Oil Chem. Soc.* **1955**, *32* (2), 49−53.
(26) Kellens, M.; Reynaers, H. Study of the Polymorphism of Saturated Monoacid Triglycerides II: Polymorphic Behaviour of a 50/50 Mixture of Tripalmitin and Tristearin. *Lipid/Fett* **1992**, *94* (8), 286−293.
(27) Himawan, C.; MacNaughtan, W.; Farhat, I. A.; Stapley, A. G. F. Polymorphic occurrence and crystallization rates of tristearin/tripalmitin mixtures under non-isothermal conditions. *Eur. J. Lipid Sci. Technol.* **2007**, *109*, 49−60.
(28) MacNaughtan, W.; Farhat, I. A.; Himawan, C.; Starov, V. M.; Stapley, A. G. F. A differential scanning calorimetry study of the crystallization kinetics of tristearin-tripalmitin mixtures. *J. Am. Oil Chem. Soc.* **2006**, *83* (1), 1−9.
(29) Lutton, E. S. The Polymorphism of Tristearin and Some of its Homologs. *J. Am. Chem. Soc.* **1945**, *67* (4), 524−527.
(30) Foubert, I.; Fredrick, E.; Vereecken, J.; Sichien, M.; Dewettinck, K. Stop-and-return DSC method to study fat crystallization. *Thermochim. Acta* **2008**, *471*, 7−13.
(31) Smith, K. W.; Bhaggan, K.; Talbot, G.; van Malssen, K. F. Crystallization of Fats: Influence of Minor Components and Additives. *J. Am. Oil Chem. Soc.* **2011**, *88* (8), 1085−1101.
(32) Siew, W.-L.; Ng, W.-L. Influence of diglycerides on crystallisation of palm oil. *J. Sci. Food Agric.* **1999**, *79* (5), 722−726.
(33) Bhaggan, K.; Smith, K. W.; Blecker, C.; Danthine, S. Binary Mixtures of Tripalmitoylglycerol (PPP) and 1,3-Dipalmitoyl-2-stearoyl- sn -glycerol (PSP): Polymorphism and Kinetic Phase Behavior. *Eur. J. Lipid Sci. Technol.* **2018**, *120* (3), No. 1700306.
(34) Yoshikawa, S.; Watanabe, S.; Yamamoto, Y.; Kaneko, F.; Sato, K. Interactive Polymorphic Crystallization Behavior in Eutectic Triacylglycerol Mixtures Containing Molecular Compound Crystals. *Cryst. Growth Des.* **2022**, *22* (3), 1753−1763.
(35) Minato, A.; Ueno, S.; Yano, J.; Wang, Z. H.; Seto, H.; Amemiya, Y.; Sato, K. Synchrotron radiation X-ray diffraction study on phase behavior of PPP-POP binary mixtures. *J. Am. Oil Chem. Soc.* **1996**, *73* (11), 1567−1572.
(36) Macridachis-González, J.; Bayés-García, L.; Calvet, A. T. An Insight into the Solid-State Miscibility of Triacylglycerol Crystals. *Molecules* **2020**, *25* (19), 4562.
(37) Vereecken, J.; Foubert, I.; Smith, K. W.; Dewettinck, K. Effect of SatSatSat and SatOSat on crystallization of model fat blends. *Eur. J. Lipid Sci. Technol.* **2009**, *111* (3), 243−258.
(38) Ahmadi, L.; Wright, A. J.; Marangoni, A. G. Chemical and enzymatic interesterification of tristearin/triolein-rich blends: Microstructure and polymorphism. *Eur. J. Lipid Sci. Technol.* **2008**, *110* (11), 1025−1034.

https://doi.org/10.1021/acs.cgd.4c01138
Cryst. Growth Des. 2024, 24, 9951−9964